The Chemical Composition and Gas-to-Dust Mass Ratio of Nearby Interstellar Matter

Priscilla C. Frisch

University of Chicago, Department of Astronomy and Astrophysics, 5460 S. Ellis Avenue, Chicago, IL 60637

Jonathan D. Slavin

Harvard-Smithsonian Center for Astrophysics, 60 Garden Street, MS 34, Cambridge, MA 02138

ABSTRACT

We use recent results on interstellar gas towards nearby stars and interstellar byproducts within the solar system to select among the equilibrium radiative transfer models of the nearest interstellar material presented in Slavin & Frisch (2002). For the assumption that O/H$\sim$400 PPM, Models 2 and 8 are found to yield good fits to available data on interstellar material inside and outside of the heliosphere, with the exception of the Ne abundance in the pickup ion and anomalous cosmic ray populations. For these models, the interstellar medium (ISM) at the entry point to the heliosphere has $n(\mathrm{H^o})$=0.202–0.208 cm^{-3}, $n(\mathrm{He^o})$=0.0137–0.0152 cm^{-3}, and ionizations χ(H)=0.29–0.30, χ(He)=0.47–0.51. These best models suggest the chemical composition of the nearby interstellar medium (ISM) is $\sim$60–70% subsolar if S is undepleted. Both $\mathrm{H^o}$ and $\mathrm{H^+}$ need to be included when evaluating abundances of ions found in warm diffuse clouds. Models 2, 8 yield an H filtration factor $\sim$ 0.46. Gas-to-dust mass ratios for the ISM towards ϵ CMa are $R_{\rm gd}= 178 - 183$ for solar abundances of Holweger (2001), or $R_{\rm gd}= 611 - 657$ for an interstellar abundance standard 70% solar. Direct observations of dust grains in the solar system by Ulysses and Galileo yield $R_{\rm gd}\simeq$115 for models 2, 8, supporting earlier results (Frisch et al. 1999). If the local ISM abundances are subsolar, then gas and dust are decoupled over small spatial scales. The inferred variation in $R_{\rm gd}$ over parsec length scales is consistent with the fact that the ISM near the Sun is part of a dynamically active cluster of cloudlets flowing away from the Sco-Cen Association. Observations towards stars within $\sim$ 500 pc show that $R_{\rm gd}$ correlates with the the percentage of the dust mass that is carried by iron, suggesting that a Fe-rich grain core remains after gain destruction. Evidently large dust grains ($> 10^{-13}$ g) and small dust grains

($< 10^{-13}$ g) are not well mixed over parsec-length spatial scales in the ISM. It also appears that very small Fe-dominated dust grains have been destroyed in the ISM within several parsecs of the Sun, since C appears to be essentially undepleted. However if gas-dust coupling breaks down over the cloud lifetime, the missing mass arguments applied here to determine $R_{\rm gd}$ and dust grain mineralogy are not appropriate.

Subject headings: ISM: abundances — ISM: clouds — dust

1. Introduction

In this paper we combine recent observations of interstellar material inside (Witte et al. 2003; Cummings et al. 2002; Gloeckler & Geiss 2003, CSS02, GG03 respectively), and outside (Gry & Jenkins 2001) of the heliosphere with radiative transfer models which predict the boundary conditions of the heliosphere (Slavin & Frisch 2002, Paper II), to evaluate the boundary conditions of the heliosphere, chemical composition of the ISM nearest the Sun, and fundamental interstellar dust properties. The precise chemical composition and physical properties of low column density ($\leq 10^{18.5}$ cm^{-2}) diffuse interstellar clouds are difficult to determine because of unobserved ionization states, component blending in distant sightlines, and unknown grain composition. The interstellar cloud surrounding the solar system provides a unique opportunity to constrain the reference abundance pattern of diffuse interstellar clouds and the composition of the gas and dust phases of the interstellar medium (ISM). For this cloud *only* we have observations over parsec length scales towards nearby stars, as well as *in situ* data sampling the cloud properties at the entry point of the heliosphere. Seaton (1951) examined the ionization equilibrium of interstellar gas towards χ^2 Ori and recognized that interstellar dust grains (ISDGs) must be included for a full understanding of the chemical composition of the ISM. Frisch et al. (1999, hereafter Paper I) found that the gas-to-dust mass ratio ($R_{\rm gd}$) in the interstellar cloud surroundign the solar system (or the Local Interstellar Cloud, LIC) falls in the range $\sim 100 - 600$ when calculated with the "missing mass" method, which compares the observed gas-phase abundances with an assumed reference chemical composition; the uncertainties reflect the poorly known ISM reference metallicity, and absorption line uncertainties.

In the special case of the interstellar cloud surrounding the solar system (the local interstellar cloud, or LIC), direct measurements of interstellar dust grains within the solar system have been obtained by the Ulysses and Galileo spacecraft, giving a second means for calculating $R_{\rm gd}$ (Paper I). The availability of two relatively direct determinations of $R_{\rm gd}$ for the LIC makes this cloud a unique laboratory for evaluating the chemical composition of our

Galaxy in general, and diffuse clouds in particular.

The LIC is a member of an ensemble of cloudlets (denoted the cluster of local interstellar clouds, CLIC) flowing from an upstream direction (after vector conversion into the local standard of rest, LSR) within ∼5° of the Galactic center and towards the Loop I supernova remnant interior. The CLIC ensemble moves through the LSR at 17.0±4.6 km s^{-1}, and the velocity dispersion represents macroscopic turbulence (Frisch et al. 2002). [1]

Observations of nearby stars sample various sightlines through the CLIC. Studies of stars with low $N(\mathrm{H^o})$ values, e.g. ϵ CMa (Gry & Jenkins 2001), REJ 1032+532 (Holberg et al. 1999) and μ Col (Howk et al. 1999), show that both neutral and ionized gas are required for accurate abundance calculations of ions formed in partially ionized clouds. Data-constrained radiative transfer models have been used to obtain both the chemical composition and ionization levels of the ISM within ∼ 3 pc (Slavin & Frisch 2002, hereafter Paper II). Such models yield gas phase abundances referenced to $\mathrm{H^o}$+$\mathrm{H^+}$, which is important when determining abundances for elements with first ionization potential (FIP) less than 13.6 eV, as well as He, Ne, and Ar and gas-to-dust mass ratios.

The ionization corrections in the radiative transfer models (Paper II) are imperative for low FIP ions in sightlines where comparable amounts of $\mathrm{H^o}$ and $\mathrm{H^+}$ exist. Clouds with $N(\mathrm{H^o}) \lesssim 10^{18.3}$ cm^{-2} will be partially ionized, since for $\mathrm{H^o}$, τ(13.6 eV)=6 for $N(\mathrm{H^o}) \sim 10^{18}$ cm^{-2}. For the partially ionized gas within ∼ 3 pc (χ(H) >20%, Paper II) both $\mathrm{H^o}$ and $\mathrm{H^+}$ must be included for abundance determinations. In particular, $\mathrm{S^+}$ exists in $\mathrm{H^o}$ and $\mathrm{H^+}$ gas. Also, Fe, Mg, Si and other refractories are significantly depleted so that neglecting $\mathrm{H^+}$ in abundance estimates for partially ionized low density clouds will yield both incorrect grain composition and inaccurate values for R_{gd}. This effect is shown by the poor correlation between $\mathrm{Fe^+}$ and $\mathrm{H^o}$ for low column densities ($\lesssim 10^{18}$ cm^{-2}, Paper I, Wakker & Mathis 2000), versus the good correlation between $\mathrm{Fe^+}$ and $\mathrm{Mg^+}$ at the lowest column densities ($N(\mathrm{Mg^+}) \lesssim 10^{12.5}$ cm^{-2}, Paper I).

Recent data on the global properties of diffuse clouds, and interstellar byproducts inside of the solar system (pickup ions,[2] PUI, neutral helium, and anomalous cosmic ray,[3] ACR)

---

[1]This direction is based on Hipparcos results, which yield a solar motion in the local standard of rest of ∼ 13.4 km s^{-1} towards the Galactic coordinates $l = 28^o$, $b = +32^o$ (Dehnen & Binney 1998). For reference, the standard solar motion yields an LSR upstream direction of $l^{\mathrm{II}} \sim 330^o$ (Frisch et al. 2002).

[2]Pickup ions are formed from the ionization of interstellar neutrals in the solar system, and subsequent Lorentz force coupling of these ions to the solar wind.

[3]Anomalous cosmic rays are formed when convected pickup ions are accelerated to energies < 300 MeV in the termination shock regions of the solar wind.

are used here to select the models best matching the combination of data on the ISM inside and outside (but nearby), the heliosphere. Paper II contains a unique approach, in that both *in situ* data and observations towards ϵ CMa are used to constrain the nearby ISM. Recent FUSE and STIS results showing a relatively constant O/H ratio in the general diffuse ISM provide additional constraints on the set of viable models from among those presented in Paper II (§2.2). The improved *in situ* data then yield two best models which are consistent with most of the data (§2.3). The implications of these models for the chemical composition of the local ISM (LISM), dust grain composition, the gas-to-dust mass ratio at the entry point to the heliosphere (§3.3), and filtration factors are also discussed. Evidence for a nearby interstellar magnetic field, which is required to maintain pressure balance with the hot gas of the Local Bubble, is discussed briefly (§3.4). A range of supplementary data are presented in the Appendix, including the interstellar ionization levels predicted for Models 2, 8, and 18.

2. Best Model for Interstellar Gas within 3 pc

Paper II presents 25 radiative transfer models of the ISM within $\sim$ 3 pc, with input variables including the neutral column density ($N(\mathrm{H^o})$) to the CLIC surface towards ϵ CMa (since it is poorly known), cloud volume density (n_{H}), and interstellar magnetic field strength (which determined the interface pressure). (For convenience, many Paper II results are plotted in the Appendix by model number.) In this section we will show that Models 2 and 8 yield the best agreement to the combined LISM data towards ϵ CMa and observations of the ISM products within the solar system. The ϵ CMa sightline was chosen for completeness of data (Gry & Jenkins 2001, §5.1), and because this star dominates the near extreme ultraviolet (EUV) radiation field (Vallerga 1996). The models were forced to produce agreement with the observed column densities of $\mathrm{C^{+*}}$, $\mathrm{N^o}$, $\mathrm{O^o}$, $\mathrm{Mg^+}$, $\mathrm{Si^+}$, $\mathrm{S^+}$, and $\mathrm{Fe^+}$ towards ϵ CMa, with no additional assumptions about elemental abundances. The combination of the observed $N(\mathrm{O^o})$ and assumed $N(\mathrm{H^o})$ presets the O abundance, since $\mathrm{O^o}$ and $\mathrm{H^o}$ ionization are tightly coupled by charge exchange (Field & Steigman 1971). Both ionization levels and abundances are predicted by the models for H, He, C, N, Mg, Si, S and Fe, and all predicted abundances were referenced to $N(\mathrm{H^o} + \mathrm{H^+})$. For Ne and Ar, the abundances are assumed to be solar abundances (see Section 2.3.1), and ionization levels are predicted by the models. These models were constrained by the interstellar column densities of clouds within 3 pc towards ϵ CMa, and interstellar cloud properties at the solar location inferred both from observations of the ISM and ISM products inside of the heliosphere.[4] The *in situ* data used in Paper II

[4]For a review of heliosphere properties see Zank (1999).

include direct observations of interstellar He^o inside of the solar system, and observations of pickup ions formed by the interaction of interstellar neutrals with the solar wind. In this paper, we also use anomalous cosmic ray Ar data (Cummings et al. 2002), produced by accelerated pickup ions, to select among models. In Paper II, we found that Models 11, 17, and 18 provided reasonable agreement with the data. Here we add information about O/H in the disk ISM, and use new data on interstellar He (Ulysses data Witte et al. 2003), pickup ions (GG03), and anomalous cosmic rays (CSS02). We will conclude below that Models 2 and 8 are the best matches to the available data from among the initial set of models presented in Paper II.

2.1. Uncertainties in the ISM Reference Abundance Pattern

Dust grains are a poorly understood reservoir of material that effectively mask the chemical composition of the ISM. Prior knowledge of the ISM reference abundance pattern in principle allows the use of volatile trace elements (e.g. S, O, N) as a hydrogen column density proxy. One possible abundance standard for the ISM is the solar system abundance pattern (Grevesse & Sauval 1998, GS98), although recent studies of the solar photosphere (Holweger 2001, H01) and solar granulation (Allende Prieto et al. 2002, Pr02) make these values less certain. Interstellar reference abundances are also poorly understood, although the subsolar B-star abundances have been suggested as a template abundance pattern for the ISM (York et al. 1983; Savage & Sembach 1996; Snow & Witt 1996; Sofia & Meyer 2001). The assumption of a solar reference abundance for the ISM can not be tested for refractory elements such as Fe, which are heavily depleted in disk and halo clouds. The reference abundances for C, N, O, S, and other elements in the ISM have been discussed extensively, including the possibility that either B-star or another subsolar abundance pattern is more appropriate as a standard for the ISM (York et al. 1983; Savage & Sembach 1996; Snow & Witt 1996; Sofia & Meyer 2001). The lower solar O/H abundances found by H01 and Pr02 remove one argument in favor of subsolar interstellar O abundances, which were needed to keep the dust-entrained O at reasonable levels (Sofia & Meyer 2001; Cartledge et al. 2001). If gas and dust are poorly mixed over subparsec distance scales (§3.3), and gas and large dust grains (radius >1 μm) are never well mixed (Gruen & Landgraf 2000), then the assumption that the ISM chemical composition is the sum of the gas and dust components will be incorrect. Our conclusion below, that the two best models favor $\sim$60–70% subsolar abundances for the LISM (§3.2), is derived independent of any assumptions about the dust composition, and is consistent with interstellar Kr results showing abundances $\sim$60% solar (or meteoritic) values (Cardelli & Meyer 1997; Cartledge et al. 2001). As a noble element, Krypton should not be depleted onto dust. However our conclusion, that abundances in the

nearby ISM are likely subsolar, conflicts with findings of solar abundances in higher column density sightlines(N(H)>10^{20} cm^{-2}) when H01 or Pr02 solar values are invoked (Sofia & Meyer 2001), so this problem is unresolved.

One possible H proxy is S^+, which is expected to be undepleted in diffuse clouds and is formed in both H^o and H$^+$gas. Towards ϵ CMa, $N(S^+) = 1.35 \times 10^{13}$ cm^{-2} (Appendix) giving log N(H)= 17.79 cm^{-2} for solar abundances (S/H = 22 PPM, from H01). Models 1, 4, 7, 10, 13, 14, 16, 17, 22, and 25 yield log $N(H^o + H^+)$ predictions that are within 0.06 dex of this value (Table 4 of Paper II), but the predicted C/H for these same models (427–832 PPM) substantially exceeds the allowed solar C/H abundances of 245–391 (GS98, H01, Pr02, Table 1). Uncertainties of $\sim$ 25% on $N(S^+)$ and 23% on the solar S/H ratio allow for agreement with several other models. We find below that Models 2 and 8 (the two best models, §2.2, §2.3) suggest that interstellar sulfur abundances in the $d < 3$ pc ISM are subsolar.

Observations of diffuse clouds in disk sightlines show that O/H is relatively constant towards stars with log $N(H^o+2H_2) < 21.5$ cm^{-2} (Cartledge et al. 2001; Andre et al. 2003). Observations of the O I λ1356 Å absorption line toward 13 stars within $\sim$500 pc, with $N(H^o+2H_2) = 1 - 2 \times 10^{21}$ cm^{-2}, and showing an average spatial density $\langle n \rangle = 0.63$ cm^{-3}, yield O/H = 347 ± 16 PPM (Meyer et al. 1998, corrected to oscillator strength $f = 1.16 \times 10^{-6}$). Observations of 19 somewhat more distant stars (1–5 kpc) with column densities $N(H^o+2H_2) \geq 10^{21}$ cm^{-2}, and an average spatial density of $\langle n \rangle = 0.38$ cm^{-3}, yield O/H = 408 ± 14 PPM (Andre et al. 2003). Both studies find that O/H is relatively constant over the sightlines sampled, although above log $N(H^o+2H_2) \sim 21.5$ cm^{-2} O depletions appear to increase. The four stars with the largest O/H ratios in the Meyer et al. sample also give averages $\langle$O/H$\rangle$ $\sim$400 PPM and $\langle n \rangle \sim 0.18$ cm^{-3}. The Andre et al. star set samples disk stars with lower average volume densities (since they are more distant) that are more similar to the $\langle n \rangle \sim 0.3$ cm^{-3} found locally. Thus we select O/H $\sim$400 PPM as a suitable value for the ISM oxygen abundance close to the Sun. This O/H abundance range is also consistent with observations of the nearby stars G191-B2B, WD0621-376, WD1634-573, WD2211-495 (to within 1σ uncertainties, Moos et al. 2002).

2.2. Selecting Models Consistent with the Disk ISM O^o/H^o

Since the H^o column density towards ϵ CMa is unknown, N(H^o) was treated as a free parameter in Paper II. In this section we will require consistency between the LISM abundance and the general disk ISM in order to narrow the selection of viable models. We assume O/H $\sim$ 400 PPM to obtain $N(H^o) = 6.5 \times 10^{17}$ cm^{-2} for the ϵ CMa sightline, since $N(O^o) = 2.6^{+0.8}_{-0.5} \times 10^{14}$ cm^{-2} (Gry & Jenkins 2001, and Appendix). For compari-

son, EUVE broadband observations found $N(\mathrm{H^o}) = 9.5 \pm 2.5 \times 10^{17}\mathrm{cm^{-2}}$ (Vallerga 1996) towards ϵ CMa, and model atmosphere calculations are consistent with an interstellar column of $N(\mathrm{H^o}) = 5 \times 10^{17}$ (Aufdenberg et al. 1998). Hence, the most viable models from Paper II are Models 2, 5, 8, 11, 18, 20 and 23, which predict O/H=380–389 PPM. Note this O abundance is 72% (H01), or 82% (Pr02) of the solar abundances (Table 1, Appendix). In the following sections (2.2 and 2.3) we argue that Models 2 and 18 are the best matches to the combined interstellar and *in situ* data. Note that none of our models have O/H∼265 PPM, as seen towards higher column density interstellar clouds Cartledge et al. (2001).

Nitrogen shows no systematic abundance or depletion variations with variable column density (York et al. 1983; Meyer et al. 1997). Towards ϵ CMa, $N(\mathrm{N^o})/N(\mathrm{H^o}) = 41 \pm 2$ PPM (for $N(\mathrm{H^o}) = 6.5 \times 10^{17}$ cm^{-2}), and the viable models (Models 2, 5, 8, 11, 18, 20 and 23) have predicted N abundances of $43.7 - 52.5$ PPM. The difference between $N(\mathrm{N^o})/N(\mathrm{H^o})$ and N/H is because N and H ionization decouples in high radiation fields. Nitrogen is dominated by charge exchange with H, except for some photoionization at the cloud surface (e.g. Fig. 2, Paper II). Meyer et al. (1997) find an interstellar abundance of 75 ± 4 PPM, however this value seems too large for diffuse clouds since FUSE observations towards low column density sightlines ($< 10^{20}$ cm^{-2}) show $N(\mathrm{N^o})/N(\mathrm{H^o}) = 35 - 60$ (Moos et al. 2002). For example, $\mathrm{N^o/H^o} = 38 \pm 8$ PPM towards HZ43 ($N(\mathrm{H^o}) \sim 8.7 \times 10^{17}$, Kruk et al. 2002); towards Capella $\mathrm{N^o/H^o} = 42 \pm 2$ PPM (Wood et al. 2002). CLIC N abundances appear to be ∼ 51%–78% of solar (Table 1). Models 2 and 8 find that N/H∼ 50, compared to H01 solar abundances of $\mathrm{N/H} = 85^{+25}_{-19}$, indicating interstellar N abundances that are ∼60% of solar values.

Sulfur is generally considered undepleted in the ISM (Savage & Sembach 1996) and S^+ is the dominant state of S in both warm neutral material and warm ionized material since FIP=10.4 eV. Neglecting H^+ yields erroneous S abundance values in partially ionized gas such as the CLIC. The restricted set of models gives a S abundance range $13.5 - 15.5$ PPM, compared to the solar abundance 22 ± 5 PPM (Table 1). Had H^+ been ignored in this low column density sightline, S would appear to have solar abundances of 21 PPM. Low interstellar S abundances are also found in HST observations of REJ1032+532, with a S abundance of 9.5 PPM (using $N(\mathrm{H^o}+\mathrm{H^+}) \sim 8 \times 10^{18}$ cm^{-2}, Holberg et al. 1999). However, the ISM towards μ Col shows solar S abundances to within uncertainties, (using $\log N(\mathrm{H^o}+\mathrm{H^+}) \sim$ 19.9 cm^{-2}, Howk et al. 1999). Based on the abundances predicted for Models 2, 5, 8, 11, 18, 20 and 23, S is present at ∼50%–90% of solar in the CLIC, with Models 2 and 8 yielding 60% solar abundances.

Nearly all C in warm diffuse clouds is singly ionized (IP=11.3 eV). Carbon abundances for the viable models are in the range 263–275 PPM, compared to solar abundances 331^{+49}_{-43} (GS98), 391^{+110}_{-86} PPM (H01), or 245^{+24}_{-21} (Pr02). Models 2 and 18, selected below as the best

models, yield C/H=263 PPM, and 309 PPM which exceeds the solar abundances found by (Pr02). The current picture of the ISM does not include supersolar C abundances in the gas phase (although poor dust-gas mixing combined with grain destruction might produce supersolar C/H gas values in small cloudlets). Thus we adopt the H01 solar abundances which imply C/H abundances that are 67%–79% solar. The mild C depletion may indicate the destruction of small dust grains, or PAHs, which is consistent with evidence that the CLIC has been shocked (Paper I). FUSE values for low column density sightlines are in the range $N(C^+)/N(H^o)= 350-800$ PPM, with large uncertainties, versus $N(C^+)/N(H^o)= 423 \pm 102$ PPM for the ϵ CMa sightline and $N(H^o)= 6.5 \times 10^{17}$ (Appendix). Including the fact that $\sim 56\%$ of the gas towards HZ43 is ionized (Kruk et al. 2002) reduces C/H to ~ 345, which is closer to the CLIC value. Model 19, which has been suggested elsewhere as the best LIC model, can be rejected since it predicts a C abundance (759 PPM) substantially larger than the solar value.

The ratios Mg^+/Mg^o and C^+/C^{+*} provide diagnostics of the cloud ionization. Among the viable models, Models 2, 8, and 18 give good agreement with Mg^+/Mg^o towards ϵ CMa (346±87), and Model 11 is consistent (Table 2). The larger predicted ratios for Mg^+/Mg^o for Models 5, 20 and 23 are inconsistent with the ϵ CMa data. The uncertainties on $N(C^+)$ are large, and all of the viable models are consistent with the observed C^+/C^{+*} ratio towards ϵ CMa to within the uncertainties. However, Models 2, 8, and 18 provide the best match. Predicted abundances for these models are compared to solar and the ISM reference abundances in Table 3. Based on these ratios and O/H$\sim$400 PPM, Models 2, 8 and 18 provide the best match to the ϵ CMa data. The Mg^+/Mg^o and C^+/C^{+*} ratios for all models, and the ionization fractions for Models 2, 8, and 18, are given in the Appendix.

2.3. Constraining Models with *in situ* Observations of the ISM

In situ observations of the products of the solar wind interaction with interstellar neutrals fed into the heliosphere by the surrounding cloud yield a sample of the ISM at the entry point to the heliosphere. The LIC is a special case because it is the only interstellar cloud with data from a single location (the entry point to the heliosphere) rather than sightline averaged values. However, *in situ* observations of interstellar neutrals and the byproducts of the ISM-heliosphere interaction introduce uncertainties from the uncertain neutral-ion interactions in the heliosheath regions between the bow shock (if it exists) and the solar wind termination shock (Ripken & Fahr 1983). These interactions have been calculated (Izmodenov et al. 1999b; Cummings et al. 2002; Müller & Zank 2002). The filtration factor, F_X for an element X, is the ratio of the densities of X^o inside and outside of the heliosphere (since

only the neutrals are able to penetrate the heliosphere). Filtration factor estimates are based on either a heliosphere model, whose boundary conditions are set by the physical properties of the ISM at the solar location, or a model of the ISM at the entry point to the heliosphere (§2.3.2). The need to decouple the calculated filtration factor from any assumptions about the heliosphere model helped to motivate this study. The most recent *in situ* data are used below to further select among the viable models. It is shown below that the pickup ion data suggest Models 2 and 8 agree best with the combined astronomical and *in situ* data.

2.3.1. Helium, Oxygen, Nitrogen, Neon, Argon

Direct observations of interstellar He^o in the solar system by Ulysses yield a temperature of 6,300±340 K and density 0.014±0.002 cm^{-3} for He at the termination shock (Witte et al. 1996, 2003). Observations of He in the pickup ion population give n(He^o)= 0.015±0.002 cm^{-3} at the termination shock (Gloeckler & Geiss 2003). We adopt n(He^o)=0.0145±0.015 cm^{-3}, which is the overlap between these independent measurements. Helium has minimal filtration ($F_{\rm He} = 0.94 - 0.99$, Table 3) in the heliosheath regions. Correcting for He^o filtration yields a LIC density at entry to the heliosphere of n(He^o)=0.013–0.017 cm^{-2}, which encompasses the predicted n(He^o) values at for Models 2, 5, 8, 11, 18 and 23. Models 2 and 8 predict n(He^o)=0.015 and 0.014 cm^{-3}.

The pickup ion data yield O^o/He^o= $(3.66 \pm 0.67) \times 10^{-3}$ for interstellar neutrals at the upstream termination shock (GG03 and Table 3). The viable models yield predictions of O^o/He^o= $(5.00 - 5.76) \times 10^{-3}$. Since over 30% of the O^o atoms may be removed by charge exchange between O^o and interstellar protons in the heliosheath regions, the predictions are consistent with the data. Comparison between the models and pickup ion data, however, do appear to rule out the augmentation of O^o in the heliosheath (or a filtration factor > 1, Müller & Zank 2002). Models 2 and 8 yield $F_{\rm O}$=0.6 for the O filtration factor (eq. 1).

The pickup ion data yield N^o/He^o= $(5.38 \pm 1.17) \times 10^{-4}$ for interstellar neutrals at the termination shock. The viable models predict N^o/He^o= $(5.11 - 6.12) \times 10^{-4}$, and these values are within the PUI uncertainties when filtration factors are included ($\sim 0.76 - 0.96$ Müller & Zank 2002; Cummings et al. 2002, Table 3). Models 2, 8, and 18 imply a N filtration factor of ~ 0.85 (eq. 1).

Neon is observed in the PUI and ACR populations, and ACR Ar is detected. As noble elements, Ne and Ar should not deplete onto dust grains, and therefore should indicate the ISM reference abundance. Both Ar^o and Ne^o are sensitive to the EUV radiation field, and the viable models predict Ar^o/Ar=22–33%, and Ne^o/Ne=9–18%. In Paper II Ne and Ar

abundances were assumed at 123 PPM and 2.82 PPM respectively. However the solar Ar abundance in GS98 is $2.51^{+0.37}_{-0.33}$ PPM, and B-star Ar abundances appear somewhat larger ($3.16^{+0.39}_{-0.34}$ PPM, Holmgren et al. 1990). In this paper we use the Holmgren Ar abundance, and correct the Paper II predictions for this 12% abundance increase.

Anomalous cosmic ray data yield $Ar^o/He^o = (1.50 \pm 0.67) \times 10^{-5}$ at the termination shock (Cummings et al. 2002; Gloeckler & Geiss 2001). Using Voyager data and new calculations of filtration factors, Cummings et al. selected Model 18 as the best match to the anomalous cosmic ray data. Below we show that Models 2 and 8 both yield satisfactory fits to the combination of ϵ CMa and *in situ* data.

Paper II noted the failure of the models to predict the pickup ion Ne values for an assumed solar abundance of 123 PPM. Neglecting Ne filtration, Models 2 and 8 predict Ne^o/He^o values that are 41–60% of the pickup ion value $Ne^o/He^o = (5.24 \pm 1.18) \times 10^{-4}$ at the termination shock (GG03, Table 3). The inclusion of Ne filtration ($\lesssim$12%) aggravates the difference between the model results and PUI Ne^o data. Models 5 and 20 predict the most Ne^o, but yield poor agreement with the ϵ CMa data. Reducing the Ne discrepancy requires either reducing Ne ionization, or raising the intrinsic interstellar abundance to $\sim$200 PPM. Since $\sim$12% of the Ne is neutral, relatively small reductions in the radiation field may raise Ne^o/He^o by the required amount. However the FIPs of Ne^o (21.6 eV) and He^o (24.6 eV) are similar, and the He^o ionization predictions are satisfactory (Table 3). An unexplored possibility is that charge exchange between He^o (ionization potential $\sim$24.6 eV) and Ne^+ in the heliosheath may amplify Ne inside of the heliosphere.

2.3.2. Hydrogen Pickup Ions and Filtration

In Paper II we did not use observations of H^o or PUI H in the solar system to constrain the models because of the poorly known but large filtration factor from charge exchange between H^o and H^+ in the heliosheath (Ripken & Fahr 1983; Izmodenov et al. 1999a). However, we now use these data to show that Models 2 and 8 provide the most consistent agreement with the PUI H data.

Following Gloeckler & Geiss (2001, GG01), assuming negligible He filtration, the filtration factor for element X can be evaluated using:

$$F_{\rm X} = \frac{n_{\rm TS}(X)/n_{\rm TS}(He)}{n_{\rm IS,Sun}({\rm X^o})/n_{\rm IS,Sun}({\rm He^o})}. \quad (1)$$

GG01 calculated the H filtration factor ($F_{\rm H}$) using pickup ion data for the H and He densities at the termination shock (TS, $n_{\rm TS}$(H) and $n_{\rm TS}$(He)), and assuming $n_{\rm IS,Sun}({\rm H^o})/n_{\rm IS,Sun}({\rm He^o}) =$

11.25 for the interstellar ratio at the entry point to the heliosphere. The value 11.25 for $n_{\rm IS,Sun}({\rm H^o})/n_{\rm IS,Sun}({\rm He^o})$ is too low for the solar location, although appropriate for sightline averaged values.[5] Paper II found sightline averaged ratios of $N({\rm H^o})/N({\rm He^o})= 8.9 - 13.6$. At the solar location, $n_{\rm IS,Sun}({\rm H^o})/n_{\rm IS,Sun}({\rm He^o})= 13.7 - 14.7$ since the H^o opacity exceeds the He^o opacity to cloud surface, yielding $F_{\rm H}$=0.45, 0.48 for Models 2, 8. Models 2, 5, 11, 18, 20, and 23 give H filtration factors in the range 0.41–0.48. The first row of Table 3 gives the model predictions for interstellar $n({\rm H^o})$ at the entry point to the heliosphere. The second row gives the interstellar $n({\rm H^o})$ calculated with a semi-empirical filtration factor applied to the pickup data $n({\rm H^o})$ at the termination shock, assuming negligible He filtration. Each of the interstellar $n({\rm H^o})$ values predicted using model-corrected filtration factors are within 15% of the $n({\rm H^o})$ value at the solar location actually predicted by the model (the first row of Table 3). Fig. 1 shows interstellar $n({\rm H^o})_{\rm is}$ derived from the PUI value at the TS corrected for filtration (ordinate, $n({\rm H^o})_{\rm is}$=$n_{\rm TS}({\rm H^o})/F_{\rm H}$)) plotted against the interstellar $n({\rm H^o})$ predicted by the models (column 10, Table 7 of Paper II). The viable models points are numbered, while the points for Model 2, 8, and 18, which are favored by the Mg and C data, are enclosed in boxes. Among the three best models favored by the ϵ CMa Mg and C data (2, 8 and 18), Models 2 and 8 yield the best self-consistency between model-predicted interstellar H^o volume densities, and model-corrected interstellar densities derived from the PUI data. Based on this comparison, we select Models 2 and 8 as the best overall matches to the available data on the LISM within ∼3 pc, and conclude that this self-consistency validates the plausibility of these results.

2.3.3. Temperature

The Ulysses observations of interstellar He^o yield a LIC cloud temperature temperature $6,300 \pm 340$ K, compared to 8,200–8,500 K predicted by Models 2 and 8. Model 25 has the lowest predicted temperature, $T= 5,120$ K, but was excluded because of unrealistically large C abundances, and disagreement with ϵ CMa ${\rm Mg^+/Mg^o}$ and ${\rm C^+/C^{+*}}$ ratios. Typical radiative recombination rates in the ISM are on the order of $T^{-2/3}$, so a predicted temperature that is too high by 1,500 K results in a recombination rate that is too small by ∼14%. Heiles (2001) concluded from comparisons of 21 cm emission and absorption that over 47% of warm

[5]It seems unlikely that a new set of model parameters with a lower initial assumed total volume density would yield a ratio close to the 11.25 value assumed by GG03. Comparisons between Models 19 and 25, which have the same input variables except for n (which is 0.273 cm^{-3}for Model 19 and 0.227 for Model 25) shows that a 27% decrease in the volume density yields a 3% increase in $n_{\rm IS,Sun}({\rm H^o})/n_{\rm IS,Sun}({\rm He^o})$ at the solar location.

neutral gas is in a thermally unstable region corresponding to 500–5000 K, a range near the LIC temperature. However, Models 2 and 8 give H ionization χ(H) ∼0.30, and n(H^o)∼0.20 cm^{-3}, and this partially ionized cloud type is in a regime not well studied theoretically.

3. Discussion

The properties Models 2, 8 and 18 are summarized in Table 4. The implications of these models are now discussed.

3.1. The Extent of the ISM towards the Nearest Stars

Models 2 and 8 give n(H^o)= 0.208 cm^{-3} and 0.202 cm^{-3} for d <3 pc ISM, based on the LISM towards ϵ CMa. If all ISM close to the Sun shares the characteristics of the LIC, then the thickness of the clouds towards nearby stars can be estimated. Towards α Cen (1.3 pc, the nearest star) log N(H^o)= 17.60−18.02 cm^{-2} (the lower limit corresponds to D/H= 1.5×10^{-5}, Linsky & Wood 1996). Thus for <n(H^o)>∼0.20 cm^{-3} (Models 2, 8), LIC-like gas would fill 60%–100% of the sightline. In the downstream direction, N(H^o)= $6.5^{+2.5}_{-2.0}$×10^{17} cm^{-2} towards Sirius AB (2.7 pc) (e.g. Hebrard et al. 1999). In this case, LIC-like gas will fill ∼37% of the sightline. Towards Procyon (3.5 pc) in the downstream direction, log N(H^o)= 18.06 cm^{-2} (for both components, Linsky et al. 1995), and a LIC-like cloud fills ∼50% of the sightline. Towards Capella (12.5 pc), the LIC gas extends ∼2.6 pc, filling ∼21% of the sightline (Table 1). Towards λ Sco (216 pc) where N(H^o)=10$^{19.23}$ cm^{-2} (York 1983), LIC-like gas extends ∼25 pc. The star λ Sco samples a sightline near the upstream CLIC direction in the LSR (Frisch et al. 2002; Frisch 1995). From this limited data sample, Models 2 and 8 suggest that LIC-like gas fills less than 50% of the sightline in downstream directions even for the nearest stars. For the upstream direction H^o data is sparse, and in addition the dispersion in cloudlet velocities and the large extent of the CLIC gas indicate that the LIC cloudlet model may not be applicable.

3.2. LISM Reference Abundances and Depletions

The chemical composition for nearby gas given by Models 2 and 8 (which provide the best overall agreement with the ISM in the ϵ CMa direction and in the heliosphere, §2.2, §2.3) is summarized in Table 1. The gas phase interstellar abundances predicted by Model 8 (Model 2) assuming no depletions are: C—275 (263); N—53 (50); by assumption O—380

(380); and S—13.2 (13.2). For C, N, O, and S, respectively, these values are 70% (67%), 62% (59%), 70%, and 60% of the H01 solar values.

Sulfur is not expected to be depleted onto dust grains in the ISM (Savage & Sembach 1996). The low S abundances found here suggest the correct reference abundance for the LISM is ∼60–70% of the H01 solar abundances. An ISM reference abundance pattern of ∼60% solar is also consistent with Kr abundances that are ∼60% solar (Cardelli & Meyer 1997).

The depletion of C onto dust grains within $\sim$ 3 pc is not required by these results, providing the abundances of the alpha-particle elements C, O, S, Kr are all subsolar by similar amounts (60–70%). Since C is a common constituent of dust grains, an interstellar gas phase abundance of ∼70 solar leaves minimal carbon for interstellar dust grains. However, Sofia & Meyer (2001) note that different elements in the ISM may have different origins. The Si, Fe, and Mg abundances are consistent with grain destruction in interstellar shocks (Paper I), so the small carbon-bearing grains (possibly PAH's) may also have been partially destroyed in the nearest interstellar gas.

The PUI and ACR populations are consistent with subsolar O and N abundances in the parent interstellar population. Models 2 and 8 match the H, He, N, O, and Ar PUI and ACR data, for reasonable filtration values. Note, however, that the uncertainties on the O, Ar and N filtration factors are comparable to the amount of subsolar LIC metallicity. The PUI and ACR Ne data are difficult to interprete in terms of the models. Filtration models predict a Ne loss of ∼12% in the heliosheath ($F_{\rm Ne} \sim 0.88$, Table 3), implying either supersolar Ne abundances in the LISM, or that the EUV radiation field is incorrect at the ionization potential of Ne (21.6 eV). Suprasolar Ne abundances are unlikely if O, N, and S abundances are subsolar. Models 2 and 8 show that Ne is 12% neutral at the solar location, so small uncertainties in Ne$^{\rm o}$ ionization levels, which are on the the EUV radiation field, will yield large variations in Ne$^{\rm o}$/Ne. This Ne discrepancy may reflect the uncertainty in the diffuse EUV radiation field, which has not been directly measured. A second possibility is that Ne$^{\rm o}$ is produced in the heliosheath, perhaps from charge exchange between Ne^{+} and He$^{\rm o}$, since He^{+} is abundant and the ionization potentials of Ne$^{\rm o}$ and He$^{\rm o}$ are within 3 eV of each other. We are unaware of any data on the cross section for this reaction so we cannot evaluate this possibility though it certainly warrants further study.

Models 2 and 8 show that Ar is ∼20% neutral at the solar location. The radiation field is poorly constrained at the FIP of Ar$^{\rm o}$ (15.8 eV, λ ∼790 Å) and highly sensitive to the cloud H$^{\rm o}$ distribution. The models and data are barely consistent if filtration is modest.

The predicted depletions for Fe, Mg, and Si for Models 2 and 8 are –1.18, –0.87, and

–0.75, compared to H01 solar values. These depletions are comparable to values between warm and cool disk cloud depletions (e.g., Welty et al. 2000). Generally most depletions are evaluated with respect to H^o rather than H^o+H^+as done here. Had only H^o been considered, these ions would be ∼0.2 dex less depleted, placing them closer to the warm disk gas (Welty et al. 2000). For an ISM abundance pattern that is 70% of solar (using H01), Models 2 and 8 predict Fe, Mg, and Si depletions of –1.02, –0.70, and –0.60 respectively. For subsolar abundances, C, N, O, and S are essentially undepleted, indicating extensive destruction of small dust grains and grain mantles in the local ISM.

3.3. Gas-to-Dust Mass Ratio

Paper I showed that $R_{\rm gd}$ determined from *in situ* observations of interstellar dust within the solar system is lower by factors of 1.5–6 when compared to $R_{\rm gd}$ determined from missing mass arguments applied to the nearby ISM. Some of the ISM data used in that paper have been updated (e.g. newer results for ϵ CMa), and we revisit the conclusions of Paper I using the results of Paper II. The $R_{\rm gd}$ predicted by applying the missing-mass arguments to the results of Models 2 and 8 is now redetermined by assuming both solar (H01, GS98) and 70% of solar abundances for the ISM abundance pattern, and including only elements listed in Tables 5 and 6. H01 solar abundances yields $R_{\rm gd}$=178 and 183 for Models 2 and 8, with the increase compared to Paper I result primarily from a ∼20% lowering of the solar O abundance. (For comparison, $R_{\rm gd}$ for Models 11, 17, and 19 gives 163, 368, and 361 using GS98 abundances.) For an ISM abundance pattern that is 70% of the H01 value, Models 2 and 8 yield $R_{\rm gd}$=611 and 657. If all trace elements heavier than He are incorporated into the dust grains, $R_{\rm gd}\sim$ 66. Uncertainties of <13% follow from the neglect of additional elements in grain mass calculations. The missing mass arguments give a sightline average value for $R_{\rm gd}$.

ISDGs from the LIC have been directly observed with detectors on board the Ulysses and Galileo satellites, where retrograde orbits characterize the interstellar versus interplanetary populations (Baguhl et al. 1996). The total dust grain mass measured by Ulysses/Galileo is 6.2×10^{-27} g cm^{-3}, extending over the mass range $3{\times}10^{-15} - 10^{-9}$ g (Paper I, Landgraf et al. 2000). This density can be compared to the interstellar gas density to obtain a second estimate of $R_{\rm gd}$ for the LIC. Models 2 and 8 yield $R_{\rm gdLIC} = 115^{+16}_{-14}$. Smaller charged grains ($< 10^{-13}$ g), which in principle sample the MRN distribution (Mathis et al. 1977), are prevented from reaching the inner solar system (∼5 AU) by Lorentz-force coupling to the solar wind as well as exclusion at the heliopause via coupling to ionized LIC gas. Thus estimates of $R_{\rm gdLIC}$ from the Ulysses/Galileo data are an upper limit to the true LIC value.

Both the B-star abundances and solar abundances are inconsistent with the direct dust measurements of $R_{\rm gdLIC}$ by Ulysses/Galileo, in agreement with the conclusions of Paper I. This difference suggests that gas and dust are not fully mixed over sub-parsec scale lengths. Gruen & Landgraf (2000) suggest that the small grain population is enriched by the destruction of larger grains which originate in a population that is not dynamically coupled to the cloud. These grains would not contribute to visual reddening, and are therefore not included in the relatively constant gas-dust ratio found from comparisons of $E(B-V)$ and H^o+H_2. The Ulysses/Galileo grains share the LIC velocity, so the large uncoupled grain destruction that may be enriching the total dust mass at the solar location happened long ago enough for the resulting grain fragments to recouple to the gas.

In the Appendix we calculate $R_{\rm gd}$ values for several clouds to nearby stars (< 500 pc) and show that $R_{\rm gd}$ is proportional to the percentage of the dust mass which is carried by Fe ($P_{\rm Fe}$). This correlation, shown in Fig. 2, indicates that grain destruction in the ISM increases $R_{\rm gd}$ by removing C, N, O, Si, and S from the grain and leaving behind an Fe-rich resiliant grain core, as found previously (e.g. Frisch et al. 1999). In §5.4 we find that $R_{\rm gd}$ for the LIC is a factor of 2–3 larger than $R_{\rm gd}$ for the blue-shifted cloud, indicating grain properties are inhomogeneous over parsec-sized scales. This grain destruction scenario has left behind Fe-rich grain cores (younger than the $\sim 10^{7-8}$ years required to replenish grain masses either through depletion onto grain surfaces or coagulation) in the LIC towards ϵ CMa. Following the arguments of Gruen & Landgraf (2000), the larger interstellar grain population observed by Ulysses and Galileo, in contrast, must consist of grain fragments small enough to couple recently to the local magnetic field, even though the parent unshattered grains and gas were not kinematically coupled. These large uncoupled grains are not counted when missing mass arguments are used to calculate $R_{\rm gd}$. Most of the mass of the interstellar dust grains detected within the solar system is carried by grains with masses $> 10^{-13}$ g (or radius > 0.2 μm), which have a gyro-radius in a weak magnetic field ($\sim$3 μG) of $\sim$0.3 pc (Gruen & Landgraf 2000). This distance is less than the distance to the LIC edge in the upstream direction. Theoretical studies predict that, because of the differences in the creation and destruction timescales for interstellar dust grains, $R_{\rm gd}$ over the small scales (such as sampled by the *in situ* data) differs from average values over longer interstellar sightlines.

Estimates of depletions in the nearby ISM using data towards 21 stars averaged together have yielded the result that the nearest ISM has $R_{\rm gd}= 73-151$, (Kimura et al. 2002), depending on the assumption of $N(H^+)/N(H^o)$. They also used somewhat different assumptions for the reference ISM standard, including solar abundances based on (Pr02) data which we have found inconsistent with our best models. Our study here (and §5.4) calculates $R_{\rm gd}$ for each individual sightline, with data on C^+, N^o, O^o, Mg^+, Si^+, and Fe^+, and in most cases S^+, so these results can not be directly compared to the Kimura et al. results.

3.4. Interstellar Magnetic Field and Cloudlet Mass

In the conductive interface model (Slavin 1989, and Paper II), magnetic pressure in the interface (balanced by the pressure of the hot plasma) is required to maintain interface EUV emission at levels which reproduce the observed ionization. Observations of the interstellar magnetic field directly outside of the heliosphere have been elusive. However, the very weak polarization of the light from nearby stars suggest a weak nearby magnetic field aligned in the plane of the Galaxy and directed towards a Galactic longitude of l $\sim$90$^{\rm o}$ (Tinbergen 1982). The ordered component of the interstellar magnetic field traced by pulsar dispersion measures suggest this field is weak ($< 3\mu$G, Frisch 1990). Figure 3 shows the electric vector polarization direction for several nearby stars sampling the Tinbergen polarization patch. The region of maximum polarization closely follows the ecliptic plane, but also coincides with the LSR upstream direction of the CLIC. The classical interstellar dust grains which cause the polarization are charged, and pile up in the heliosheath regions as they are deflected around the heliosphere (Paper I), so they were not sampled by the Ulysses/Galileo satellites. The pileup of "classical" interstellar grains in the heliosheath regions might possibly contribute to the weak polarization observed by Tinbergen.

A magnetic field in the Galactic plane would be tilted with respect to the ecliptic by $\sim$60$^{\rm o}$. The north ecliptic pole is directed towards l=96$^{\rm o}$, b=30$^{\rm o}$, giving an ecliptic plane tilted by $\sim$60$^{\rm o}$ with respect to the Galactic plane. Observations by Voyager 1 and 2 of a dozen $\sim$3 kHz emission events in the outer heliosphere also suggest that the interstellar magnetic field direction is parallel to the Galactic plane (Kurth & Gurnett 2003).

The relatively good correlation between interstellar gas (H$^{\rm o}$ + H_2) and color excess ($E(B-V)$) indicates that gas and dust are coupled on scales of $\sim$100 pc or greater (Bohlin et al. 1978). The CLIC gas towards ϵ CMa, summing the two cloudlets together, is very low mass. Models 2 and 18 can be used to estimate the mass of these cloudlets, treating them as a single spherical cloudlet. This cloudlet extends $< 10,000$ AU towards α Cen ($\sim$ 30$^{\rm o}$ from the LIC LSR upstream direction), and $\sim$ 1 pc towards ϵ CMa. Assuming a nominal cloud diameter of 1 pc, as consistent with data, the cloudlet mass is then $\sim$0.003 $M_\odot$.

3.5. Origins of LIC

The abundance pattern of refractory elements in the CLIC has been used as an indicator of cloud origin (Frisch 1981). The abundances of Si, Mg and Fe in the CLIC gas are consistent with grain processing through a shock of velocity $\sim$ 100 km s^{-1} (Paper I).

Frisch (1979, 1981) proposed that the nearest ISM originated from the asymmetric expansion of a supershell, whose kinematics were dominated by material flowing from higher density star formation regions into the lower density regions of the Local Bubble, and the refractory elements in the CLIC are consistent with processing through a $\sim$ 100 km s^{-1} shock front (Paper I). An alternative scenario is that the CLIC originated as an outflow of material evaporated from dense clouds in the Scorpius star formation region (Frisch 1995), although this does not explain enhanced refractory abundances. An alternative scenario is that the nearby ISM results from Rayleigh-Taylor unstable material ejected from the "interface" between the Local Bubble and Loop I where grains would also have been shocked (Breitschwerdt et al. 2000). The bulk ISM flow past the Sun has velocity in the Local Standard of Rest of -17 ± 5 km s^{-1}, from the upstream direction $l \sim 2.3^{o}$, $b \sim -5.2^{o}$(Frisch et al. 2002). For all of these scenarios, the star formation epochs in the Sco-Cen Association are younger than the timescales for replenishing dust grains, so the grain destruction processes have not yet been balanced by grain growth locally.

4. Conclusions

The primary conclusions of this paper are as follows:

1. By using line of sight data towards nearby stars (including *FUSE* and STIS data, Moos et al. 2002; Andre et al. 2003) combined with observations of the ISM interaction products inside of the solar system to choose among radiative transfer models, we are able to select two models which yield very good fits to available data. These models make a range of predictions, including the chemical composition of the ISM near the Sun, the filtration factor for H^{o} entering the solar system, and the physical properties of the interstellar cloud surrounding the solar system. The most definitive discriminants among models turned out to be the global O/H ratio ($\sim$400 PPM), Mg^{+}/Mg^{o} towards ϵ CMa, and the H^{o}/He^{o} ratios inside and outside of the solar system. Both H^{o} and H^{+} need to be included when evaluating abundances of ions found in warm diffuse clouds.

2. We find that the two best models (Models 2 and 8 of Paper II) indicate that the chemical composition of the nearest ISM is likely to be subsolar, or $\sim$ 70% of the H01 solar values. This conclusion rests primarily on the inferred S abundance under the assumption that S is undepleted, and the assumed O abundance which yields good matches between ISM data inside and outside of the heliosphere.

3. For these same two models, the filtration factor for H^{o} in the heliosheath regions is $\sim$ 0.46. Filtration factors for N ($\sim$ 0.85) and O ($\sim$ 0.6) are also predicted (§2.3).

4. We show that these models give gas-to-dust mass ratios calculated for the nearest ISM towards ϵ CMa from the missing mass method of $R_{\rm gd}= 178 - 183$, provided that the chemical composition of the nearest ISM is solar. We note that for this model to be viable S must be incorporated into dust. This $R_{\rm gd}$ value differs by nearly a factor of two from the $R_{\rm gd}$ calculated directly from Ulysses and Galileo observations of interstellar dust grains in the solar system ($R_{\rm gd}\simeq 115$, consistent with Frisch et al. 1999). This result is consistent with predictions that the differences in the creation and destruction timescales for interstellar dust grains will cause $R_{\rm gd}$ to vary over sub-parsec length scales (Dwek 1998; Hirashita 1999), and the fact that the ISM near the Sun is part of a dynamically active cluster of cloudlets flowing away from the Sco-Cen Association (Frisch et al. 2002).

5. We show that the assumption of solar abundances also yields a grain composition whereby the percentage of the dust mass that is carried by iron is directly correlated to $R_{\rm gd}$ (§5.4). The implication is that the Fe forms a robust core that is not destroyed during grain processing in the ISM. Since dust mass is proportional to the ISM metallicity Dwek (1998), this apparent correlation deserves further investigation.

6. For an ISM reference standard that is 70% of H01 solar values, as is indicated by our Models 2 and 8, the $R_{\rm gd}$ ratio is raised by a factor of three to $R_{\rm gd}$=611–657. In this case we infer a dust composition of primarily Fe, Mg and Si. The correlation between $R_{\rm gd}$ and the Fe fraction of the dust mass is preserved for this case, although $R_{\rm gd}$ values are increased.

7. Comparisons between *in situ* dust data and these results suggest nearby interstellar gas and dust haven't been fully coupled over the lifetime of the cloud. If either gas-dust coupling breaks down over the cloud lifetime, or if refractory elements are also present in subsolar abundances, then applying missing mass arguments to determine dust grain mineralogy will not work.

8. The neon abundance remains a problem for these models, which may indicate either incorrect solar abundances, incorrect ionization correction (due to a poorly understood EUV radiation field), or possibly unmodeled charge exchange between interstellar He^{o} and Ne^{+} in the heliosheath regions.

These results are encouraging since they show that radiative transfer models based on accurate interstellar radiation field data, and combined with precise ISM measurements towards nearby stars and inside the heliosphere, offer the possibility of understanding the detailed physics of the ISM and the interaction between the heliosphere and the ISM. However, the conclusion that Models 2 and 8 are the best models is sensitive to the data uncertainties.

This paper as originally submitted used data from Gloeckler & Geiss (2001, private communication) and Witte et al. (1996, private communication). During the extended refereeing process newer data became available and are incorporated into this paper. The differences between the H and He densities in the earlier data and the values used here are <10%, yet this difference is large enough to replace Model 18 (as originally concluded) with Model 8 (as found here) as one of the two best models.

The authors would like to gratefully acknowledge research support from NASA grants, including NAG5-6405, and NAG5-11005, and NAG5-8163. We thank Alan Cummings, Ed Stone, George Gloeckler, Hans Mueller, Gary Zank, Dan Welty, and Don York for many helpful discussions.

REFERENCES

Allende Prieto, C., Lambert, D. L., & Asplund, M. 2002, ApJ, 573, L137

Andre, M., Oliveira, C., Howk, J. C., Ferlet, R., Desert, J. M., aHebrard, G., Lacour, S., Lecavelier des Etangs, A., Vidal-Madjar, A., & Moos, H. W. 2003, ApJ, in press

Aufdenberg, J. P., Hauschildt, P. H., Shore, S. N., & Baron, E. 1998, ApJ, 498, 837

Baguhl, M., Grun, E., & Landgraf, M. 1996, Space Science Reviews, 78, 165

Bohlin, R. C., Savage, B. D., & Drake, J. F. 1978, ApJ, 224, 132

Breitschwerdt, D., Freyberg, M. J., & Egger, R. 2000, A&A, 361, 303

Cardelli, J. A. & Meyer, D. M. 1997, ApJ, 477, L57

Cardelli, J. A., Savage, B. D., & Ebbets, D. C. 1991, ApJ, 383, L23

Cartledge, S. I. B., Meyer, D. M., Lauroesch, J. T., & Sofia, U. J. 2001, ApJ, 562, 394

Cummings, A. C., Stone, E. C., & Steenberg, C. D. 2002, ApJ, 578, 194

Dehnen, W. & Binney, J. J. 1998, MNRAS, 298, 387

Dwek, E. 1998, ApJ, 501, 643

Federman, S. R., Sheffer, Y., Lambert, D. L., & Gilliland, R. L. 1993, ApJ, 413, L51

Field, G. B. & Steigman, G. 1971, ApJ, 166, 59

Frisch, P. C. 1979, ApJ, 227, 474

—. 1981, "Nature", 293, 377

Frisch, P. C. 1990, in Physics of the Outer Heliosphere, ed. S. Grzedzielski & D. E. Page, 1st COSPAR Colloquium, Warsaw, 19–22

—. 1995, Space Sci. Rev., 72, 499

Frisch, P. C., Dorschner, J. M., Geiss, J., Greenberg, J. M., Grün, E., Landgraf, M., Hoppe, P., Jones, A. P., Krätschmer, W., Linde, T. J., Morfill, G. E., Reach, W., Slavin, J. D., Svestka, J., Witt, A. N., & Zank, G. P. 1999, ApJ, 525, 492

Frisch, P. C., Grodnicki, L., & Welty, D. E. 2002, ApJ, 574, 834

Gloeckler, G. & Geiss, J. 2001, in AIP Conf. Proc. 598: Joint SOHO/ACE workshop "Solar and Galactic Composition", 281–+

Gloeckler, G. & Geiss, J. 2003, Advances in Space Research, in press

Grevesse, N. & Sauval, A. J. 1998, Space Science Reviews, 85, 161

Gruen, E. & Landgraf, M. 2000, J. Geophys. Res., 105, 10291

Gry, C. & Jenkins, E. B. 2001, A&A, 367, 617

Hebrard, G., Mallouris, C., Ferlet, R., Koester, D., Lemoine, M., Vidal-Madjar, A., & York, D. 1999, A&A, 350, 643

Heiles, C. 2001, ApJ, 551, L105

Hirashita, H. 1999, A&A, 344, L87

Holberg, J., Bruhweiler, F., & Dobie, M. B. P. D. 1999, ApJ, 517, 841

Holmgren, D. E., Brown, P. J. F., Dufton, P. L., & Keenan, F. P. 1990, ApJ, 364, 657

Holweger, H. 2001, in AIP Conf. Proc. 598: Joint SOHO/ACE workshop "Solar and Galactic Composition", 23–+

Howk, J. C., Savage, B. D., & Fabian, D. 1999, ApJ, 525, 253

Izmodenov, V. V., Geiss, J., Lallement, R., Gloeckler, G., Baranov, V. B., & Malama, Y. G. 1999a, J. Geophys. Res., 104, 4731

Izmodenov, V. V., Lallement, R., & Geiss, J. 1999b, A&A, 344, 317

Kimura, H., Mann, I., & Jessberger, E. K. 2002, ApJ, accepted

Kruk, J. W., Howk, J. C., André, M., Moos, H. W., Oegerle, W. R., Oliveira, C., Sembach, K. R., Chayer, P., Linsky, J. L., Wood, B. E., Ferlet, R., Hébrard, G., Lemoine, M., Vidal-Madjar, A., & Sonneborn, G. 2002, ApJS, 140, 19

Kurth, W. S. & Gurnett, D. A. 2003, J. Geophys. Res., in press, 000

Landgraf, M., Baggaley, W. J., Grün, E., Krüger, H., & Linkert, G. 2000, J. Geophys. Res., 105, 10343

Linsky, J. L., Diplas, A., Wood, B. E., Brown, A., Ayres, T. R., & Savage, B. D. 1995, ApJ, 451, 335

Linsky, J. L. & Wood, B. E. 1996, ApJ, 463, 254

Müller, H. & Zank, G. P. 2002, "Solar Wind 10: AIP Conference Proceedings"

Mathis, J. S., Rumpl, W., & Nordsieck, K. H. 1977, ApJ, 217, 425

Meyer, D. M., Cardelli, J. A., & Sofia, U. J. 1997, ApJ, 490, L103

Meyer, D. M., Jura, M., & Cardelli, J. A. 1998, ApJ, 493, 222

Moos, H. W., Sembach, K. R., Vidal-Madjar, A., York, D. G., Friedman, S. D., Hébrard, G., Kruk, J. W., Lehner, N., Lemoine, M., Sonneborn, G., Wood, B. E., Ake, T. B., André, M., Blair, W. P., Chayer, P., Gry, C., Dupree, A. K., Ferlet, R., Feldman, P. D., Green, J. C., Howk, J. C., Hutchings, J. B., Jenkins, E. B., Linsky, J. L., Murphy, E. M., Oegerle, W. R., Oliveira, C., Roth, K., Sahnow, D. J., Savage, B. D., Shull, J. M., Tripp, T. M., Weiler, E. J., Welsh, B. Y., Wilkinson, E., & Woodgate, B. E. 2002, ApJS, 140, 3

Morton, D. C. 1975, ApJ, 197, 85

Ripken, H. W. & Fahr, H. J. 1983, A&A, 122, 181

Savage, B. D., Cardelli, J. A., & Sofia, U. J. 1992, ApJ, 401, 706

Savage, B. D. & Sembach, K. R. 1996, ARA&A, 34, 279

Seaton, M. J. 1951, MNRAS, 111, 368

Slavin, J. D. 1989, ApJ, 346, 718

Slavin, J. D. & Frisch, P. C. 2002, ApJ, 565, 364

Snow, T. P. & Witt, A. N. 1996, ApJ, 468, L65

Sofia, U. J. & Meyer, D. M. 2001, ApJ, 554, L221

Tinbergen, J. 1982, A&A, 105, 53

Vallerga, J. 1996, Space Sci. Rev., 78, 277

Wakker, B. P. & Mathis, J. S. 2000, ApJ, 544, L107

Welty, D. E., Hobbs, L. M., Lauroesch, J. T., Morton, D. C., Spitzer, L., & York, D. G. 2000, ApJS, 124, 465

Witte, M., Banaszkiewicz, M., & Rosenbauer, H. 1996, Space Sci. Rev., 78, 289

Witte, M., Banaszkiewicz, M., Rosenbauer, H., & McMullin, D. 2003, Adv. Space Res, in press, 0000, 0000

Wood, B. E., Redfield, S., Linsky, J. L., & Sahu, M. S. 2002, ApJ, 581, 1168

York, D. G. 1983, ApJ, 264, 172

York, D. G., Spitzer, L., Jenkins, E. B., Bohlin, R. C., Hill, J., Savage, B. D., & Snow, T. P. 1983, ApJ, 266, L55

Zank, G. P. 1999, Space Science Reviews, 89, 413

5. Appendix

5.1. ϵ CMa Data

The column densities for the d<3 pc LIC and blue-shifted clouds towards ϵ CMa were summed together in Paper II, since both clouds appear to contribute to the attenuation of the interstellar radiation field. The resulting column densities (from Paper I) are: $N(\mathrm{C}^+)= 2.1 - 3.4 \times 10^{14}$ cm^{-2}, $N(\mathrm{C}^{+*})= 1.5 \pm 0.31 \times 10^{12}$ cm^{-2}, $N(\mathrm{N}^{\mathrm{o}})= 2.68 \pm 0.1 \times 10^{13}$ cm^{-2}, $N(\mathrm{O}^{\mathrm{o}})= 2.6^{+0.8}_{-0.5} \times 10^{14}$ cm^{-2}, $N(\mathrm{Mg}^+)=4.15 \pm 0.11 \times 10^{12}$ cm^{-2}, $N(\mathrm{Mg}^{\mathrm{o}})=1.2 \pm 0.3 \times 10^{10}$ cm^{-2}, $N(\mathrm{Si}^+)= 6.37 \pm 0.3 \times 10^{12}$ cm^{-2}, $N(\mathrm{S}^+)= 1.35 \pm 0.36 \times 10^{13}$ cm^{-2}, and $N(\mathrm{Fe}^+)= 1.87 \pm 0.1 \times 10^{12}$ cm^{-2}.

5.2. Solar Abundances

Solar abundances have been established by GS98, using a combination of photospheric, corona, and meteoritic abundances. (Abundances are summarized in Table 1.) Photospheric data provide C (331 ± 49 PPM), N (83 ± 12 PPM), and O (676 ± 100 PPM) abundances. Less precise coronal data give Ne (120 ± 18 PPM) and Ar (2.51 ± 0.37 PPM). H01 updated the photospheric abundances, obtaining new C (391 ± 110 PPM), N (85 ± 25 PPM), O (545 ± 107 PPM), and Neon (100 ± 17 PPM) abundances. Pr02 considered solar granulation and found solar C, N and O abundances lower than those of GS98 or H01 for C (245^{+24}_{-21} PPM), O (490^{+136}_{-97} PPM), and for N (68 PPM).

C, N, O. Holmgren et al. (1990) determined B-star Ar abundances of $3.16^{+0.39}_{-0.34}$, which is larger than, but within the uncertainties of, the solar abundance (Table 1). In this paper we adopt H01 and GS98 values for solar abundances with the H01 values given priority.

5.3. Model Predictions

The predictions of the 25 models in Paper II are shown, by model number, in Figs. 4–6. Fig 4 shows the ionization diagnostics, Mg^+/Mg^o and C^+/C^{+*}, for each model, and the value towards ϵ CMa. Models 2, 8, and 18 provide the best fit to both the Mg and C ionization diagnostics. The predicted abundances (in PPM) for S, C, N, and O are shown in Fig. 5. The interstellar O abundance is plotted as dashed lines.

Fig. 6 shows the model predictions for He, Ar, Ne, O, N, and T at the entry point to the heliosphere. The uncertainties on these observation values are the *in situ* data are also shown. The Ar values differ from values in Paper II because an abundance of 3.16 PPM is used.

5.4. Gas-to-Dust Mass Ratio towards Nearby Stars

For Fig. 2, $R_{\rm gd}$ was calculated as described in §3.3 and Frisch et al. (1999). References for the data used to construct Fig. 2 are as follows: warm and cold clouds towards ζ Oph (Savage & Sembach 1996; Savage et al. 1992; Cardelli et al. 1991; Federman et al. 1993; Morton 1975), η UMa (Frisch et al. unpublished), λ Sco (York 1983), and 23 Ori (both 'WL' and 'SL' components Welty et al. 2000), and the LIC and blue-shifted clouds towards α CMa (Hebrard et al. 1999), and ϵ CMa (Gry & Jenkins 2001). Capella results are also included (Wood et al. 2002). For all of these clouds, data on C^+, N^o, O^o, Mg^+, Si^+, and

Fe^+ are available, and in most cases also S^+ data. In some cases, H^o and H^+ were estimated from ionization indicators such as N^o and N^+, while towards the two CMa stars the two individual clouds were assumed to have ionization levels predicted by Models 2 and 8. The bottom plot shows R_{gd} values calculated for an assumed chemical composition standard that is equal to the solar abundance pattern (using H01, when available, and GS98 abundances). The top plot shows R_{gd} values calculated using a reference standard in the ISM that is 70% of the solar values. The correlation between R_{gd} and the percentage of grain mass carried by Fe appears to indicate that grain destruction increases R_{gd} and leaves behind an iron-rich grain core. The clouds with $P_{Fe} > 25$ include the LIC clouds towards Sirius and ϵ CMa, λ Sco, ζ Oph warm cloud, and the two clouds towards 23 Ori. All of these clouds have a known origin in star-formation regions, and except for the 23 Ori SLV cloud, relatively large velocities ($|V| > 15$ km s^{-1}) in the LSR. The blue-shifted clouds towards Sirius and ϵ CMa have $P_{Fe} < 25$, and show R_{gd} values that are factors of 2–3 less than for the LIC. Evidently grain destruction is minimized in blue-shifted cloud, suggesting different origins for the LIC and blue-shifted clouds (e.g. Frisch 1995). Note that He is included in gas-mass estimates, and O^o and N^o abundances are referenced to H^o alone for calculating the points shown in Fig. 2.

5.5. Predicted Ionization Levels for Models 2, 8, and 18

The ionization levels predicted for H, He, C, N, O, Ne, Na, Mg, Al, Si, P, S, Ar,Ca, and Fe by Models 2, 8, and 18 are listed in Tables 5, 6, and 7.

Table 1. Abundances: Solar, ISM, and Models[a]

Element	Solar Reference Abundance[b]			(X_{tot}/H_{tot} from SF02[c] Models)							X^n/H^o in Gas Phase ISM[d]				
	GS98	H01	Pr02	2	5	8	11	18	20	23	Ion	Ref.	ϵ CMa[f]	Capella[g]	HZ43[h]
C	331^{+49}_{-43}	391^{+110}_{-86}	245^{+24}_{-21}	263	339	275	331	309	398	380	C^+	141^{+21e}_{-18}	423±102	363::	794::
N	83^{+12}_{-11}	85^{+25}_{-19}	∼68	50.1	46.8	52.5	47.9	49.0	43.7	45.7	N^o	75±4[e]	41±2	42±2	38±8
O	676^{+100}_{-87}	545^{+107}_{-90}	490^{+60}_{-53}	380	389	380	389	389	389	389	O^o	375±47[j]	[400±126]	490::	380±87
Ne	120^{+18}_{-16}	100^{+17}_{-15}	···	[123]	···	···	···	···	···	···	···	···	···	···	···
Mg	38^{+5}_{-4}	35^{+5}_{-4}	···	4.68	5.25	4.90	5.37	5.37	5.62	5.75	Mg^+	···	6.4±0.2	3.7	3.0
Si	34±4	34±4	···	6.03	6.76	6.03	6.61	6.61	7.08	6.92	Si^+	···	10±1	5.34	8.3
S	21^{+6}_{-5}	22±5	···	13.2	14.5	13.2	14.5	14.5	15.5	15.1	S^+	···	21±6	<23	···
Ar	$2.51^{+0.37}_{-0.33}$	···	$(3.16^{+0.39}_{-0.34})$	[2.82]	···	···	···	···	···	···	Ar^o	···	···	<18	1.1
Fe	$31.6^{+3.9}_{-3.4}$	28^{+6}_{-5}	···	1.86	2.04	1.86	2.00	2.04	2.14	2.09	Fe^+		2.9±0.2	1.8	1.7

[a]All abundances are given in parts per million H atoms (PPM).

[b] Solar abundances are from Grevesse & Sauval (1998, GA98), Holweger (2001, H01), and Allende Prieto et al. (2002, Pr02). The Ar abundance enclosed in parentheses in the Pr02 column is from B-star abundances determined by Holmgren et al. (1990).

[c] The SF02 models (columns 5-11) present ISM abundances with respect to H^o+H^+ for the ϵ CMa sightline. Model abundances in brackets are assumed and invariant between the models.

[d] The "Reference" column refers to global ISM studies which include dense cloud sightlines. Interstellar values marked with "::" have uncertainties on the order of 100%.

[e] Reference ISM abundances from Sofia & Meyer (2001, C, N).

[f]Based on $N(H^o)$=6.5 x 10^{17} cm^{-2}.

[g]Data from Wood et al. (2002).

[h]Data from Kruk et al. (2002), using curve of growth values in Table 5.

[i]Based on $N(H^o)$=6.37 x 10^{17} cm^{-2}, from O/H=408.

[j]We combine O/H=408±14 PPM (Andre et al. 2003), and O/H=343±15 from GHRS data (Meyer et al. 1998) to obtain the listed value 375±47 (§2.2).

Table 2. Ionization Diagnostics[a]

Ratio	Value[b]	SF02 Models[c]						
		2 *	5	8 *	11	18 *	20	23
Mg^{+}/Mg^{o}	346±87	351.0	515.8	316.4	428.7	341.9	819.3	560.6
C^{+}/C^{+*}	183±58	182.4	211.5	185.4	210.5	190.9	236.2	230.3

[a] Abundances given in parts per million H atoms (PPM).

[b] For the combined LIC and blue-shifted cloud in the ϵ CMa sightline.

[c] Best models based on ϵ CMa Mg and C data.

Table 3. Interstellar Gas at Solar Location: *In situ* Data versus Models

Quantity	Results[1]	Ref.	Model Predictions (no filtration)							Filtration[2]
			2	5	8	11	18	20	23	
H^o (cm^{-3})	0.095±0.01	4	0.208	0.225	0.202	0.212	0.242	0.228	0.216	0.40, (0.43)
H^o		6	0.213	0.213	0.236	0.218	0.228	0.203	0.209	From text
He^o (cm^{-3})	0.0145±0.0015	3,4	0.015	0.017	0.014	0.016	0.017	0.018	0.017	0.99, 0.94
N^o/He^o	(5.38±1.17)E-4	4	5.63E-4	5.49E-4	6.12E-4	5.53E-4	5.92E-4	5.11E-4	5.28E-4	0.96, 0.76
O^o/He^o	(3.66±0.67)E-3	4,5	5.34E-3	5.29E-3	5.76E-3	5.45E-3	5.65E-3	5.00E-3	5.20E-3	1.17, 0.70
Ne^o/He^o	(5.24±1.18)E-4	4	2.85E-4	3.18E-4	2.37E-4	2.62E-4	2.62E-4	3.50E-4	2.79E-4	0.87, 0.88
Ar^o/He^o	(1.50±0.67)E-5	5,4	1.07E-5	1.27E-5	1.08E-5	1.20E-5	1.25E-5	1.40E-5	1.30E-5	0.90, 0.64
Temperature (K)	6,300±340	3	8,230	7,750	8,480	8,080	8,140	7,200	7,750	

[1] "E-n" indicates multiplication by 10^{-n}.

[2] Filtration factors are from Müller & Zank (2002); Cummings et al. (2002, Model 1, upwind TS), and Izmodenov et al. (1999b, H^o only). The filtration factors for ratios refer to the numerator (the He^o filtration is not repeated). The H^o filtration factor in parentheses is derived in the text from Model 18.

[3]The listed $n(He^o)$ value is the average of the Ulysses and pickup ion (next note) measurements of $n(He^o)$. The final values from the 12-year Ulysses mission observations of interstellar $n(He^o)$ in the solar system give a velocity vector of 26.3±0.4 km s^{-1} towards downstream direction λ=74.7±0.5°, β=–5.2±0.2°, corresponding to an upstream direction of l^{II}=3.3°, b^{II}=+15.9° (Witte et al. 2003).

[4]Pickup ion data are values at the termination shock from GG03.

[5]Anomalous cosmic ray data from Cummings et al. (2002), for values at termination shock.

[6]These values for $n(H^o)$ are derived using the filtration factor formula of Gloeckler & Geiss (2001), with $n_{IS,Sun}$ values from the models. See Section 2.3.2.

Table 4. Results of Models

Quantity	Model 2	Model 8	Model 18
Assumed Parameters :			
$n_{\rm H}$ (cm^{-3})	0.273	0.273	0.300
log $T_{\rm h}$ (K)	6.0	6.1	6.1
$B_{\rm o}$ (μG)	5.0	5.0	3.0
$N_{\rm HI}$ (10^{17} cm^{-2})	6.5	6.5	6.5
FUV Field[a]	MMP	MMP	GPW
Predicted Properties for ISM at Solar Location :			
n(H$^{\rm o}$) (cm^{-3})	0.208	0.202	0.242
n(He$^{\rm o}$) (cm^{-3})	0.016	0.014	0.017
n(e$^-$) (cm^{-3})	0.098	0.10	0.089
χ(H$^{\rm o}$)[b]	0.287	0.30	0.234
χ(He$^{\rm o}$)	0.471	0.51	0.448
T (K)	8,230	8,480	8,140
$R_{\rm gd}$– Ulysses/Galileo Data	103	113	
Predicted Properties for ISM in ϵ CMa Sightline :			
log N(H$^{\rm o}$ + H$^+$) (cm^{-2})	18.03	18.02	17.98
N(H$^{\rm o}$)/N(He$^{\rm o}$)	11.6	12.7	12.1
$R_{\rm gd}$–Solar Abundances[c]	178	183	198
$R_{\rm gd}$–ISM Abundances[c]	611	657	669

[a]MMP→Mathis et al. 1983;
GPW→Gondhalekar et al. 1980.

[b]χ(X) is the ionization fraction of element X.

[c]The assumed solar abundances are from Holweger (2001, see text). The ISM reference abundance is assumed at 70% of the Holweger (2001) solar values.

Table 5. Model 2 Predictions for Ionization Fractions at the Sun[a]

Element	Abundance (ppm)	Ionization Fraction I	II	III	IV
H	1.00E+06	0.714	0.287	0.00	0.00
He	1.00E+05	0.521	0.471	0.00838	0.00
C	263.	0.000457	0.968	0.0319	0.00
N	50.1	0.586	0.414	0.000213	0.00
O	380.	0.733	0.267	0.000124	0.00
Ne	123.	0.121	0.646	0.233	6.23E-06
Na	2.04	0.00143	0.889	0.109	4.09E-06
Mg	4.68	0.00214	0.825	0.173	0.00
Al	0.0794	7.46E-05	0.974	0.0173	0.00894
Si	6.03	4.64E-05	0.997	0.00336	3.19E-05
P	0.219	0.000173	0.976	0.0234	0.000102
S	13.2	8.51E-05	0.961	0.0384	3.01E-06
Ar	2.82[b]	0.199	0.488	0.313	6.22E-06
Ca	0.000407	2.92E-05	0.0178	0.982	0.000211
Fe	1.86	0.000198	0.967	0.0332	9.59E-06

[a]Model 2 from Slavin & Frisch (2002).

[b]This is the Ar abundance used in Paper II. In this paper we use Ar/H=3.16 PPM from Holmgren et al. (1990).

Table 6. Model 8 Predictions for Ionization Fractions at the Sun[a]

Element	Abundance (ppm)	Ionization Fraction I	II	III	IV
H	1.00E+06	0.701	0.299	0.00	0.00
He	1.00E+05	0.475	0.511	0.0141	0.00
C	275.	0.000449	0.961	0.0382	0.00
N	52.5	0.554	0.446	0.000296	0.00
O	380.	0.721	0.279	0.000169	0.00
Ne	123.	0.0916	0.610	0.298	1.06E-05
Na	2.04	0.00122	0.848	0.151	3.90E-06
Mg	4.90	0.00232	0.791	0.206	0.00
Al	0.0794	7.85E-05	0.973	0.0180	0.00900
Si	6.03	4.80E-05	0.996	0.00401	3.39E-05
P	0.219	0.000177	0.972	0.0276	0.000124
S	13.2	8.71E-05	0.955	0.0454	4.46E-06
Ar	2.82[b]	0.182	0.469	0.349	9.23E-06
Ca	0.000407	3.33E-05	0.0181	0.982	0.000289
Fe	1.86	0.000225	0.965	0.0353	1.27E-05

[a]Model 18 from Slavin & Frisch (2002).

[b]This is the Ar abundance used in Paper II. In this paper we use Ar/H=3.16 PPM from Holmgren et al. (1990).

Table 7. Model 18 Predictions for Ionization Fractions at the Sun[a]

Element	Abundance (ppm)	Ionization Fraction I	II	III	IV
H	1.00E+06	0.766	0.234	0.00	0.00
He	1.00E+05	0.538	0.448	0.0135	0.00
C	309.	0.000407	0.971	0.0287	0.00
N	49.0	0.650	0.350	0.000141	0.00
O	389.	0.782	0.218	7.93E-05	0.00
Ne	123.	0.115	0.618	0.268	8.14E-06
Na	2.04	0.00146	0.842	0.156	3.48E-06
Mg	5.37	0.00211	0.786	0.212	0.00
Al	0.0794	7.69E-05	0.973	0.0179	0.00940
Si	6.61	4.98E-05	0.997	0.00239	2.84E-05
P	0.219	0.000174	0.977	0.0227	9.94E-05
S	14.5	8.44E-05	0.960	0.0396	3.42E-06
Ar	2.82[b]	0.240	0.473	0.287	5.08E-06
Ca	0.000407	2.71E-05	0.0164	0.983	0.000230
Fe	2.04	0.000206	0.974	0.0255	6.83E-06

[a]Model 18 from Slavin & Frisch (2002).

[b]This is the Ar abundance used in Paper II. In this paper we use Ar/H=3.16 PPM from Holmgren et al. (1990).

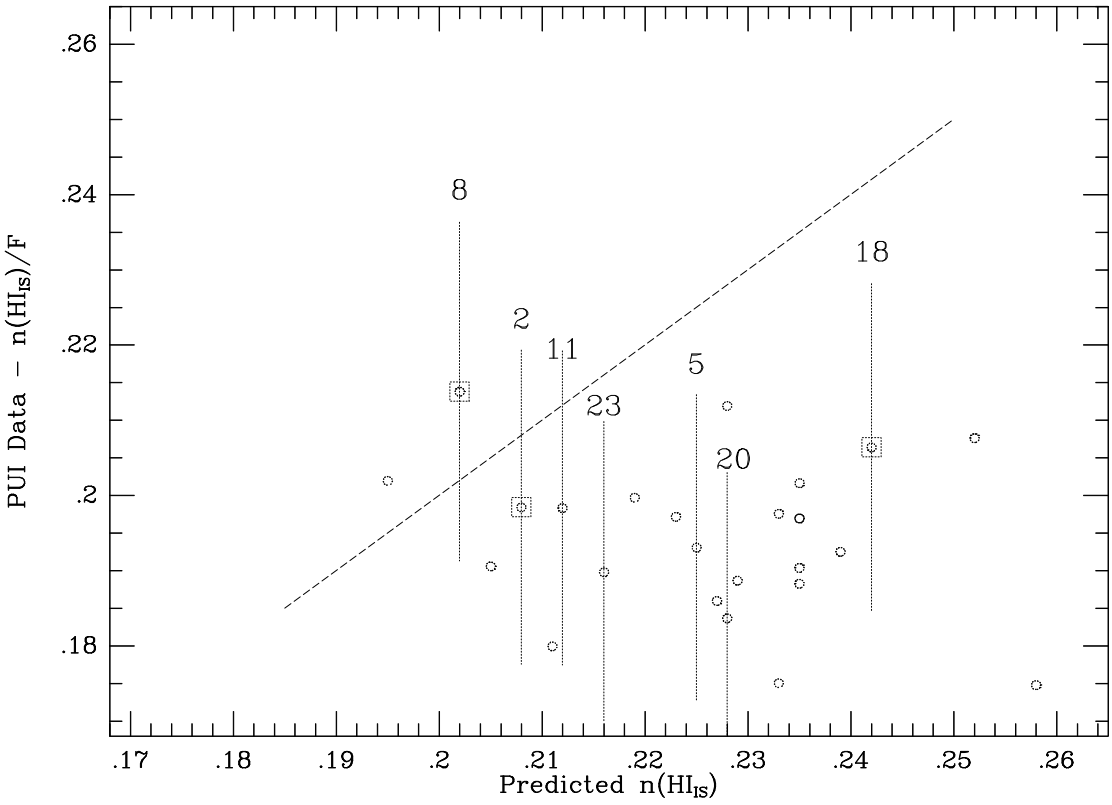

Fig. 1.— Comparison between H^{o} in the pickup ion population and model predictions for n(H^{o}) for the 25 models. The ordinate is the interstellar n(H^{o}) value that results after the pickup ion measurement of n(H^{o}) at the termination shock is corrected for heliosheath filtration (see text). The abscissa is the predicted n(H^{o}) at the solar location. The viable models show the uncertainties due to the pickup ion data, and the three best models based on Mg^{+}/Mg^{o} and C^{+}/C^{+*} ratios have boxes around the data points. (The points for Models 16 and 17, which differ only in the FUV radiation field, are superimposed on each other.)

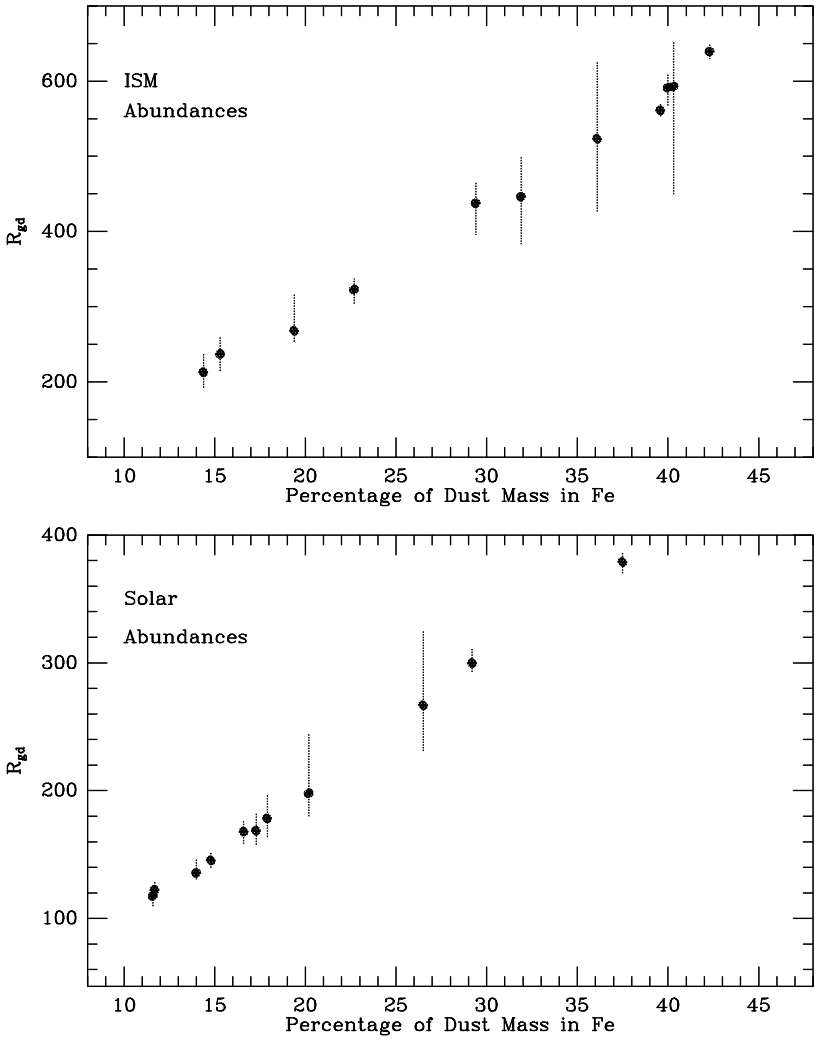

Fig. 2.— Plot of the gas-to-dust mass ratio ($R_{\rm gd}$) versus the percentage of dust grain mass carried by iron, towards a set of clouds seen towards relatively nearby stars. The uncertainties on $R_{\rm gd}$ values are shown. Data for clouds towards ζ Oph (both warm and cold clouds), η UMa, Capella, λ Sco, and 23 Ori (both 'WL' and 'SL' components) are plotted. The LIC and blue-shifted components towards Sirius and ϵ CMa are also plotted. The bottom plot shows $R_{\rm gd}$ values calculated for a reference standard in the ISM that is equal to solar abundances (using H01 and GS98 abundances). The top plot shows $R_{\rm gd}$ values calculated for a reference standard that is 70% of solar values in the ISM. The Appendix (§5.4) lists the data sources for this plot.

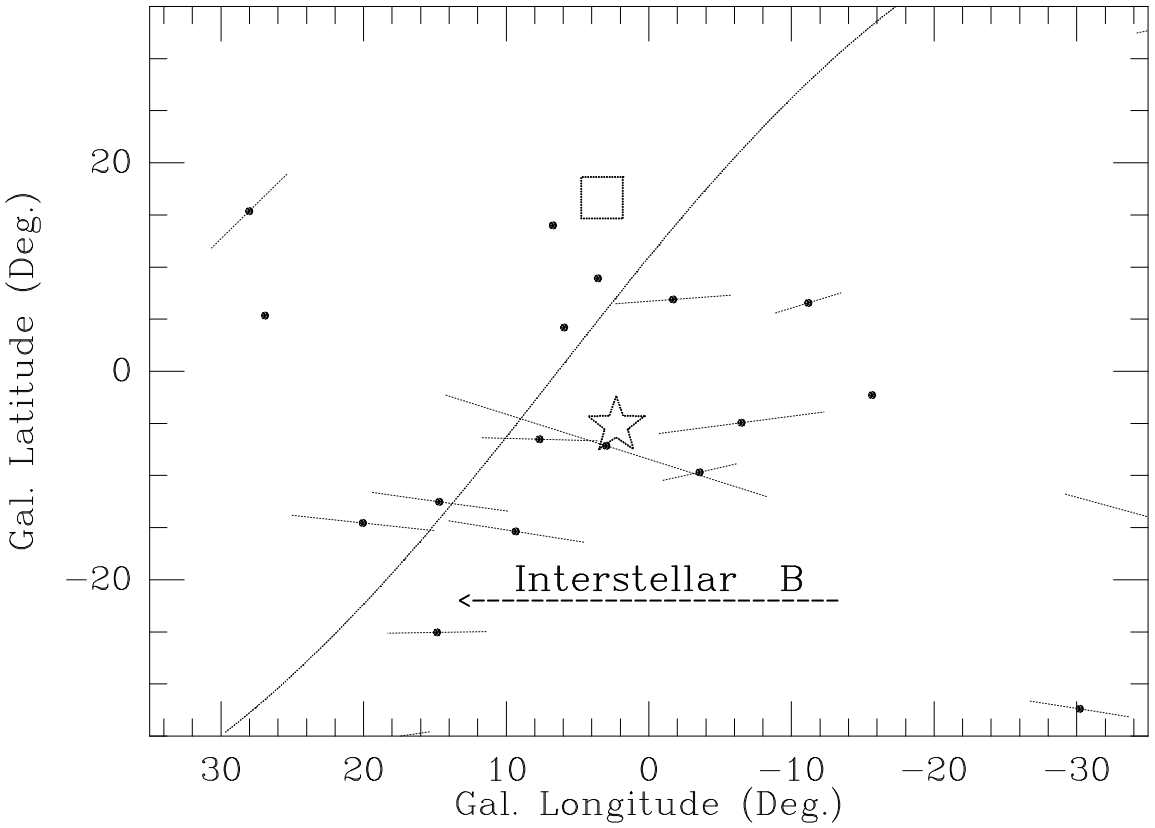

Fig. 3.— Plot of an indicator of the nearby interstellar magnetic field, in galactic coordinates. The bars show the direction of the electric vector polarization, which is parallel to the interstellar magnetic field direction, for several nearby stars (Tinbergen 1982). The arrow shows the likely direction of the interstellar magnetic field near the Sun based on this data. The curved line shows the ecliptic plane. The region of maximum polarization follows the ecliptic plane. The classical interstellar dust grains which polarize optical radiation pile up in the heliosheath regions as they are deflected around the heliosphere (Frisch et al. 1999). The box shows the heliosphere nose direction in heliocentric coordinates, and the star shows the CLIC bulk flow upstream direction in the the local standard of rest (see text).

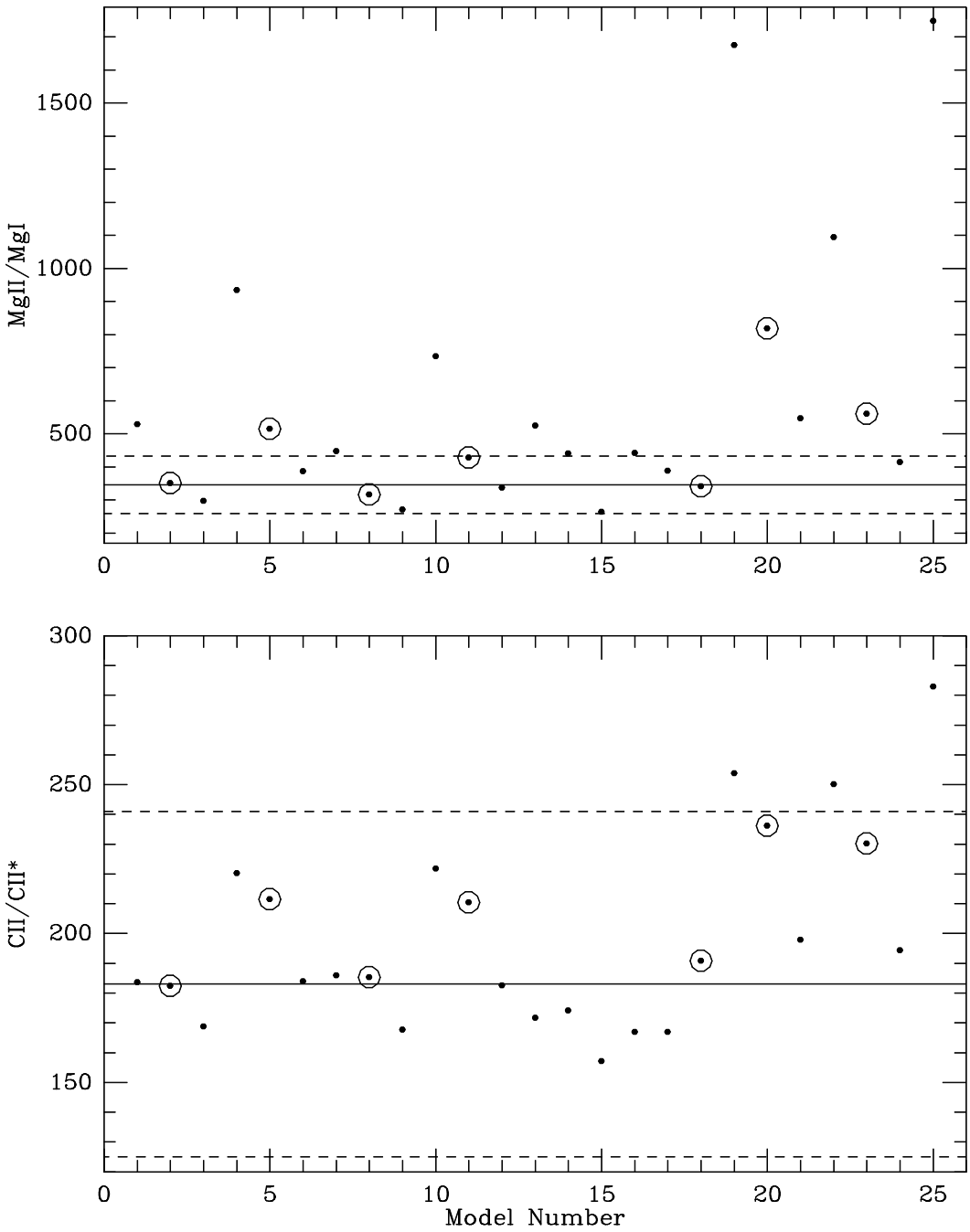

Fig. 4.— Predicted $N(Mg^+)/N(Mg^o)$ (top) and $N(C^+)/N(C^{+*})$ (bottom) plotted against model number. The observed ratios towards ϵ CMa are plotted as lines (with the uncertainties plotted as dashed lines). The models consistent with O/H$\sim$400 PPM are circled.

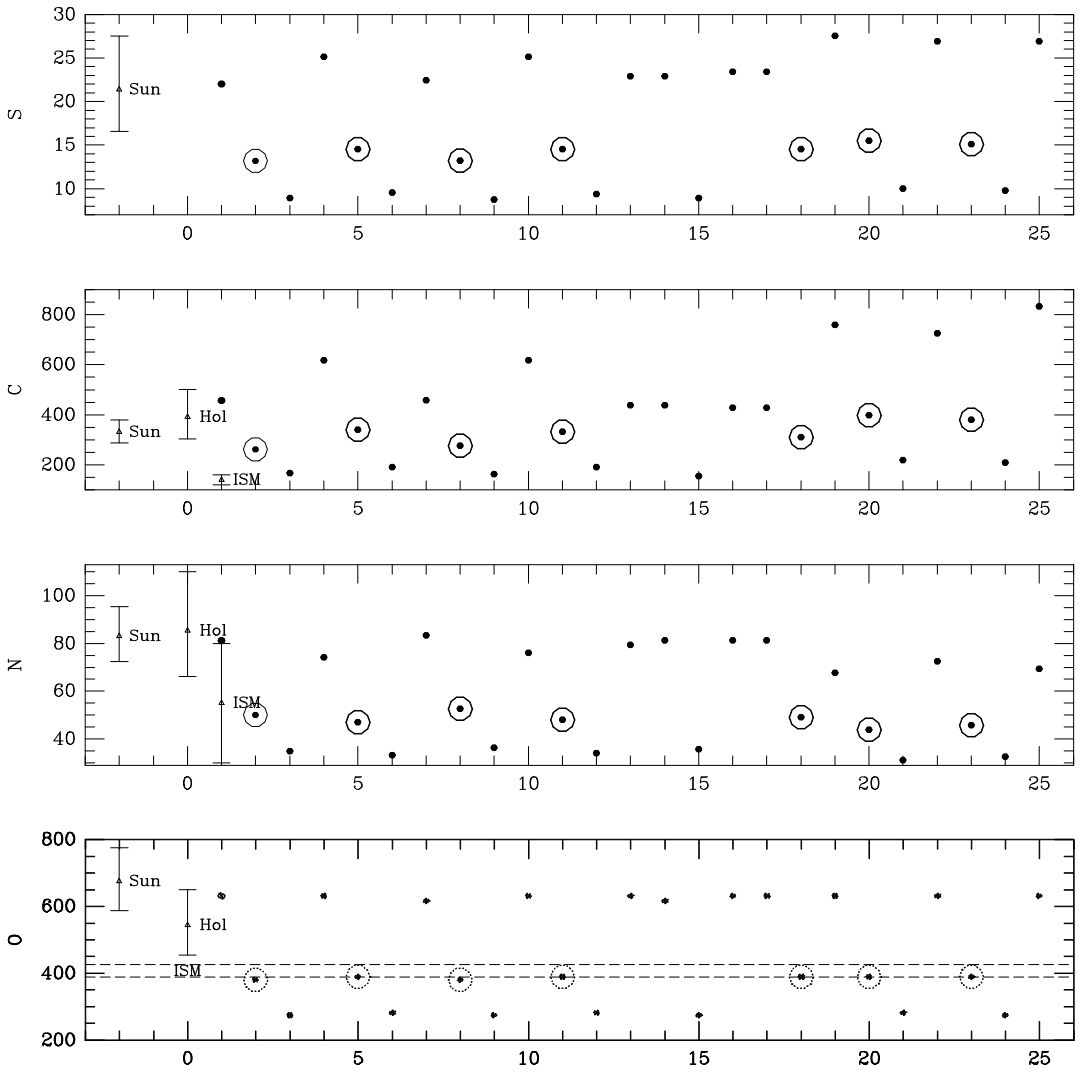

Fig. 5.— Plot of S, C, N, and O (top to bottom) abundances predicted for the 25 Models, shown in PPM versus model number. Comparison abundances are shown for solar abundances (Sun, GS98), H01 abundances and the ISM values (Andre et al. 2003; Sofia & Meyer 2001). The models consistent with O/H∼400 PPM are circled.

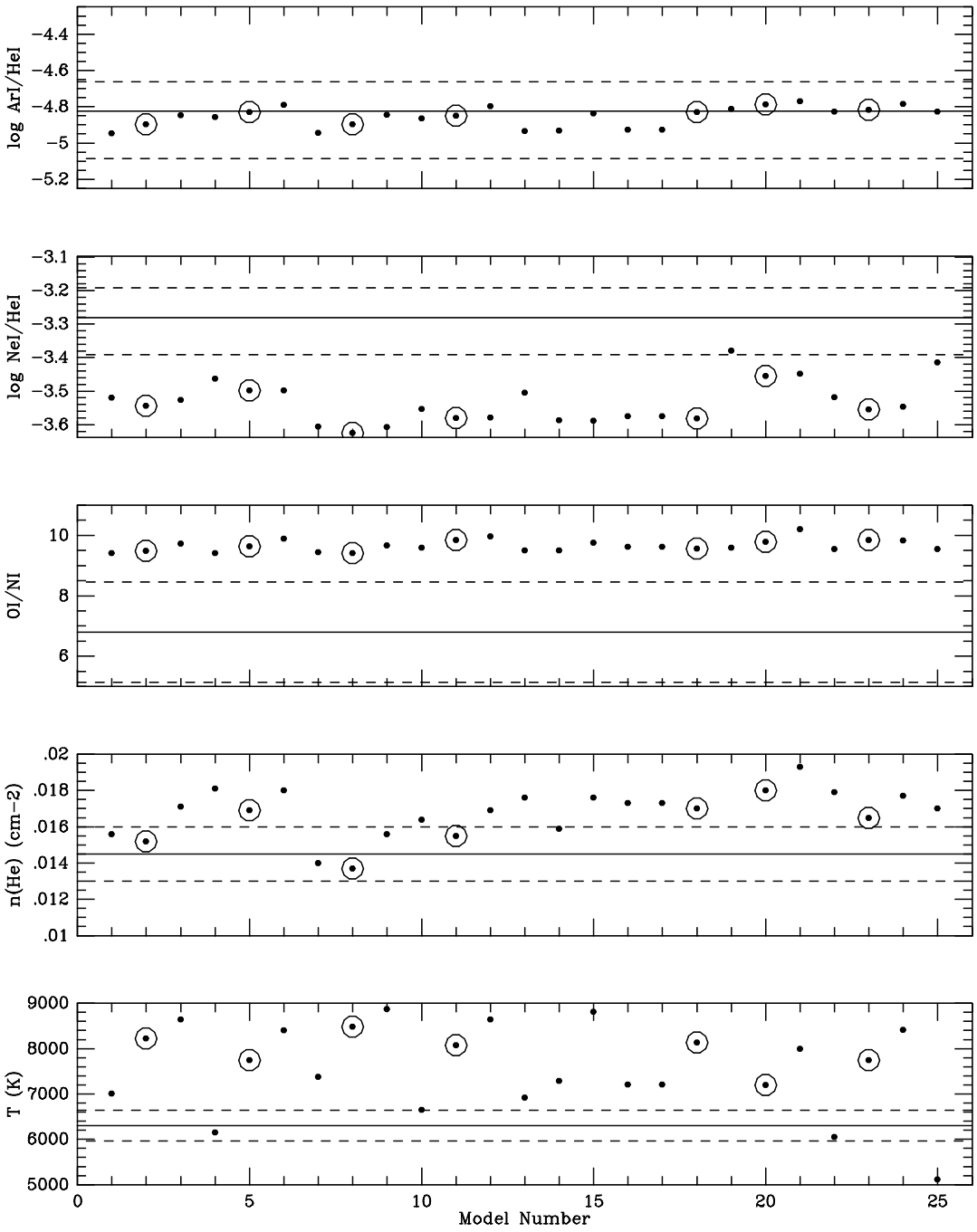

Fig. 6.— Predicted quantities for the solar location are plotted against model number. The comparison data, which includes pickup ion, direct observations of He^o, and anomalous cosmic ray data (Table 3), are plotted as lines (with uncertainties shown as dashed lines.) Top to bottom: $\log(Ar^o/He^o)$, $\log(Ne^o/He^o)$, O^o/N^o, $n(He^o)$, and temperature. The models consistent with O/H∼400 PPM are circled.